


Surround modulation is predominantly orientation-unspecific in macaque V1

Xing-Nan Zhao^{a,b,1}, Sheng-Hui Zhang^{a,b,1}, Shi-Ming Tang^{c,d,*}, Cong Yu^{a,d,**} 

^a School of Psychological and Cognitive Sciences, Peking University, Beijing, Beijing, China

^b PKU-Tsinghua Center for Life Sciences, Peking University, Beijing, China

^c School of Life Sciences, Peking University, Beijing, China

^d IDG-McGovern Institute for Brain Research, Peking University, Beijing, China

ARTICLE INFO

Keywords:

Surround modulation
Orientation
Population gain control
V1
Macaque
Two-photon imaging

ABSTRACT

Surround modulation is a fundamental property of V1 neurons, playing critical roles in stimulus integration and segregation. It is believed to be orientation-specific, as neurons' responses at preferred orientations are suppressed more by iso-oriented surrounds than by cross-oriented surrounds. Here, we investigated an alternative hypothesis that surround modulation is primarily orientation-unspecific, in that the observed "orientation-specific" surround effects actually reflect overall gain changes that affect neurons tuned to all orientations. We employed two-photon calcium imaging to compare V1 population orientation tuning functions under iso- and cross-surround modulation in awake, fixating macaques. While confirming "orientation-specific" surround suppression in individual neurons, our analysis of the population orientation tuning functions revealed that iso-surrounds induce a general orientation-unspecific suppression across all orientation-tuned neurons, plus weak orientation-specific suppression to neurons tuned to the center stimulus orientation. Furthermore, cross-surrounds mainly reduce orientation-unspecific suppression by scaling up responses of all orientation-tuned neurons. These findings suggest a model of population gain control where surround stimuli mostly scale the responses of the neuronal population. Further population coding analyses supported this conclusion, demonstrating that surround suppression leads to degraded target orientation information at least partially due to a reduced number of contributing neurons with diverse orientation preferences.

1. Introduction

Responses of V1 neurons to stimuli presented within the classical receptive field are strongly influenced by stimuli in the surrounding area, known as the non-classical receptive field (Hubel and Wiesel, 1965; Blakemore and Tobin, 1972; Gilbert, 1977; Knierim and van Essen, 1992; Cavanaugh et al., 2002a). Historically, single-neuron recording studies have shown that surround modulation is primarily orientation-specific (Blakemore and Tobin, 1972; Knierim and van Essen, 1992; DeAngelis et al., 1994; Li and Li, 1994; Kastner et al., 1997). For instance, the peak responses of individual V1 neurons to high-contrast line stimuli presented within the classical receptive field are more significantly suppressed by iso-oriented surrounding lines than by cross-oriented ones (Knierim and van Essen, 1992). These orientation-dependent response changes have also been observed in psychophysical studies (Polat and Sagi, 1993; Yu and Levi, 2000; Chen

and Tyler, 2002; Yu et al., 2003), and are associated with perceptual saliency and visual popout effects (Knierim and van Essen, 1992; Kastner et al., 1997; Li, 1999).

The observed orientation specificity of surround suppression suggests that it is at least partially mediated by long-range horizontal connections (Gilbert et al., 1996; Li, 1999; Stettler et al., 2002; Adesnik, Bruns et al., 2012; Shushruth et al., 2012; Angelucci et al., 2017). Particularly prevalent in the superficial layers of V1, these intralaminar axonal projections (Gilbert and Wiesel, 1989; Malach et al., 1993; Bosking, Zhang et al., 1997) create a network that links neurons with similar orientation preferences, allowing for the integration of information across larger areas of the visual field. As a result, they likely form the circuit basis for the generation of orientation-specific surround modulation.

However, several recent studies have indicated that V1 horizontal connections may also target heterogeneous orientation domains,

* Corresponding author at: School of Life Sciences, Peking University, Beijing, China.

** Corresponding author at: School of Psychological and Cognitive Sciences, Peking University, Beijing, China.

E-mail addresses: tangshm@pku.edu.cn (S.-M. Tang), yucong@pku.edu.cn (C. Yu).

¹ Equal-contribution first authors.

especially over longer distances beyond the classical receptive field (Chavane et al., 2011; Huang et al., 2014; Martin et al., 2014; Omer et al., 2019; Ju et al., 2020). For example, our own dendrite imaging study revealed that V1 neurons receive heterogeneous orientation inputs, as locally clustered inputs at different dendrite tree spots represent different orientation domains (Ju et al., 2020). These findings raise an important question: Is surround modulation genuinely orientation-specific as commonly believed, or is it indicative of a more general effect that is predominantly orientation-unspecific? In the latter case, the observed orientation-specific surround modulation could simply arise because a surround stimulus exerts maximal suppression on neurons responding most strongly to a stimulus at their preferred orientation.

To test this alternative hypothesis, we studied neuronal population responses to iso- and cross-surround modulation in the V1 of macaques using two-photon calcium imaging. Utilizing a customized macaque two-photon imaging setup (Li et al., 2017), we recorded the responses of approximately 1000 superficial-layer V1 neurons within each response field of view (FOV). We were particularly interested in how the population orientation tuning function, which incorporates the responses of neurons tuned to all orientations, was affected by iso- and cross-surrounds. We reasoned that if surround modulation is orientation-specific, we would observe its effects primarily in the segment of the population orientation tuning function around the center stimulus orientation. Conversely, if the modulation is orientation-unspecific, we would expect the entire population orientation tuning function to be scaled uniformly. Our findings from population response averaging and decoding generally support the hypothesis of a largely orientation-unspecific nature of surround modulation.

2. Materials and methods

2.1. Monkey preparation

Monkey preparations were identical to those reported in previous studies (Guan et al., 2021; Ju et al., 2021). Three rhesus monkeys (*Macaca mulatta*) aged 4–6 years were each prepared with two sequential surgeries under general anesthesia and strictly sterile conditions. In the first surgery, a 20-mm diameter craniotomy was performed on the skull over V1 (Fig. 1A). The dura was opened, and multiple tracks of 100–150 nL AAV1.hSynap.GCaMP5G.WPRE.SV40 (AV-1-PV2478, titer 2.37×10^{13} (GC/ml), Penn Vector Core) were pressure-injected at a depth of $\sim 350 \mu\text{m}$ at multiple locations. To ensure uniform expression of GCaMP, the injection sites were spaced approximately 1 mm apart. The dura was then sutured, the skull cap was re-attached with three titanium lugs and six screws, and the scalp was sewn up. After the surgery, the animal was returned to the cage and treated with injectable antibiotics (Ceftriaxone sodium, Youcare Pharmaceutical Group, China) for one week. Postop analgesia was also administered. The second surgery was performed 45 days later. A T-shaped steel frame was installed for head stabilization, and an optical window was inserted onto the cortical surface. Data collection could start as early as one week later. More details of the preparation and surgical procedures can be found in Li et al. (2017). The procedures were approved by the Institutional Animal Care and Use Committee, Peking University.

2.2. Behavioral task

After a ten-day recovery from the second surgery, monkeys were seated in primate chairs with a head restraint. They were trained to hold fixation on a small white spot (0.2°) with binocular viewing. The eye positions were monitored by an Eyelink-1000 eye tracker (SR Research) at a sampling rate of 1000-Hz. During the experiment, trials with the eye position deviated 1.5° or more from the fixation before stimulus offset

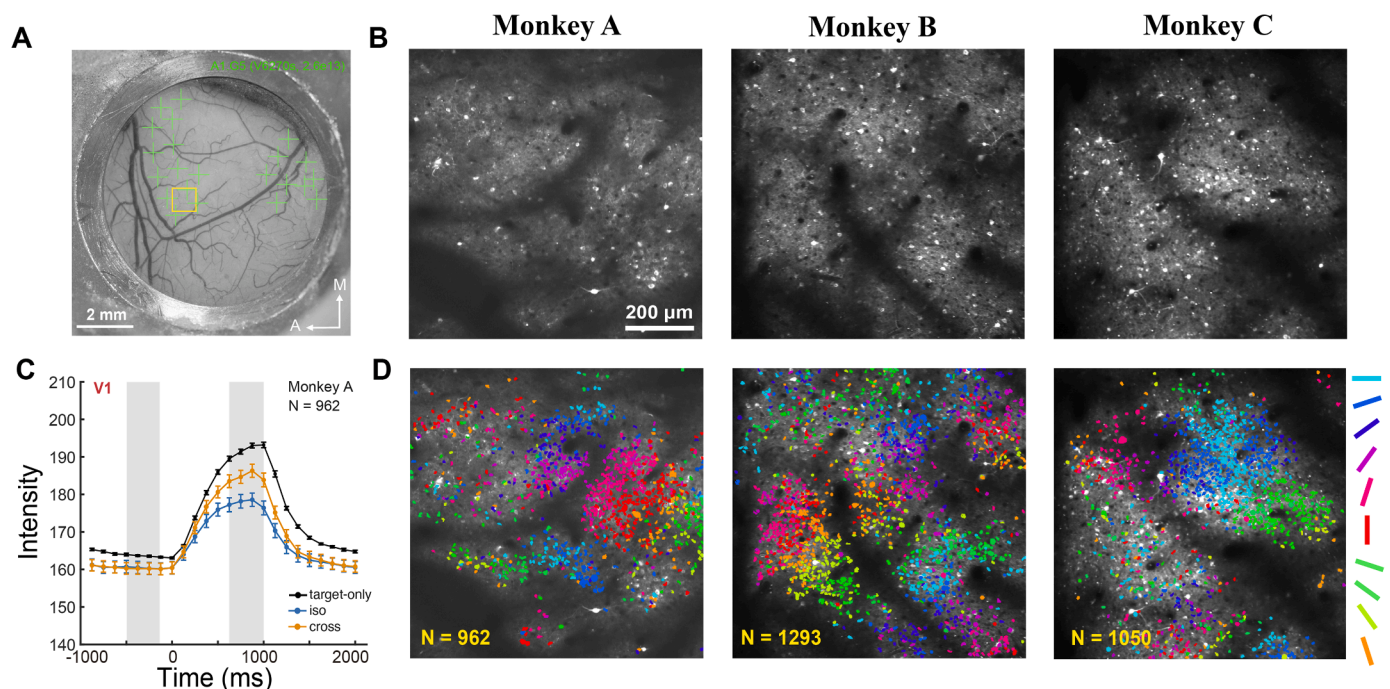


Fig. 1. Two-photon calcium imaging and orientation functional maps. A. The exemplar vascular map of an optical window in Monkey A. Green “+” signs indicate the viral injection regions. Yellow boxes on vascular maps indicate the FOV chosen for two-photon imaging ($850 \times 850 \mu\text{m}^2$). A - anterior; M - medial; B. Average 2-photon images at a cortical depth of $\sim 200 \mu\text{m}$ over a recording session for each FOV. C. Exemplar time courses of calcium responses in a FOV from Monkey A. The orange and blue curves are averaged across all orientation-tuned V1 neurons responding to the target-only, iso-surround, and cross-surround conditions, respectively. Each dot indicates the response intensity with one frame (8 frames per second after averaging every 4 frames). Error bars represent ± 1 SEM. Shaded areas before or after the stimulus onset in each plot denote 4 frames that were used for calculating the F_0 and F values, respectively. D. Orientation functional maps of FOVs.

were discarded and repeated. For the remaining trials, the eye positions were mostly concentrated around the fixation point. We checked the eccentricities of fixations under target-only and surround conditions in Monkey C (Fig. S1). Fixations were within a radius of 0.50° from the central fixation for 95 % of the time under target-only conditions and 97.5 % of the time under surround conditions. More specifically, the mean deviation was $0.250^\circ \pm 0.136^\circ$ (mean \pm SD) from the fixation point under target-only conditions and $0.215^\circ \pm 0.102^\circ$ under surround conditions. Therefore, the monkey maintained stable fixations equally well with or without the surround stimuli.

2.3. Visual stimuli and experimental design

Visual stimuli were generated by a Matlab-based Psychtoolbox-3 software (Pelli and Zhang, 1991) and presented on an Acer XB271HU monitor (refresh rate = 80 Hz, resolution = 2560 pixel \times 1440 pixel, and pixel size = 0.23 mm \times 0.23 mm). The screen luminance was linearized by an 8-bit look-up table, and the mean luminance was 18 cd/m². The viewing distance was 100 cm.

A drifting square-wave grating (3 cycles/s, full contrast, 4 cpd spatial frequency, and 0.4° diameter in size) was used to determine the population receptive field (pRF) location and approximate size associated with a specific FOV. The same stimulus was also monocularly presented to confirm the V1 location as ocular dominance columns would appear. This fast process used a 4 \times objective lens mounted on the two-photon microscope and did not provide cell-specific information. The recorded V1 pRF was centered at $\sim 1.6^\circ$ eccentricity in Monkey A, $\sim 0.9^\circ$ in Monkey B, and $\sim 3.5^\circ$ in Monkey C. All pRFs were approximately circular in shape with a diameter of $\sim 0.9^\circ$.

The experimental center-surround stimuli were formed by identical Gabors drifting at a speed of 2 cycles/sec with a contrast at 0.9. Given that most neurons preferred spatial frequencies of 4–8 cpd in Monkeys A and B (as determined in a separate study), the spatial frequency of each

Gabor was set at 6 cpd for all three monkeys. The stimulus configuration consisted of a target Gabor centered in pRF with 1–3 surround rings placed outside the pRF. The surround consisted of 1–3 rings of Gabors, each with the same spatial frequency and size as the central Gabor but with potentially different orientations. These rings were formed by 6, 12, and 18 equally spaced Gabors, with center-to-center distances of approximately 0.96° , 1.92° , and 2.88° from the central Gabor, respectively. To investigate the orientation-specific surround modulation on V1 neurons, the center Gabor was rotated from 0° to 162° in 18° steps, while the surround orientation was fixed at 0° or 90° , resulting in the center-surround orientation contrasts ranging from 0° to 162° . The center-surround orientation contrast at 0° was denoted as the iso-surround condition, while at 90° as the cross-surround condition (Fig. 2A). The stimuli were viewed through a circular opening ($r = \sim 14^\circ$) of black cardboard that covered the rest of the screen.

Each stimulus was presented for 1000 ms during recording, followed by an inter-stimulus interval (ISI) of 1500 ms, which is sufficient to allow the calcium signals back to the baseline level (Guan et al., 2018). Each stimulus condition was repeated 12–14 times. Imaging of neuronal responses to all pseudo-randomly presented stimulus conditions for a specific FOV was completed in a single session that lasted 2–3 hours (only including the recording time). During the task, the monkey could close its eyes for rest anytime when it felt tired and struggled to hold a stable gaze. These periods of rest were not included in the recording time.

2.4. Two-photon calcium imaging

Two-photon calcium imaging (Fig. 1B) was performed with a Prairie Ultima IV (In Vivo) two-photon microscope (Prairie Technologies), along with a Ti:sapphire laser (Mai Tai eHP, Spectra Physics). GCaMP5 was chosen as the indicator of calcium signals because the fluorescence activities it expresses are linearly proportional to neuronal spike

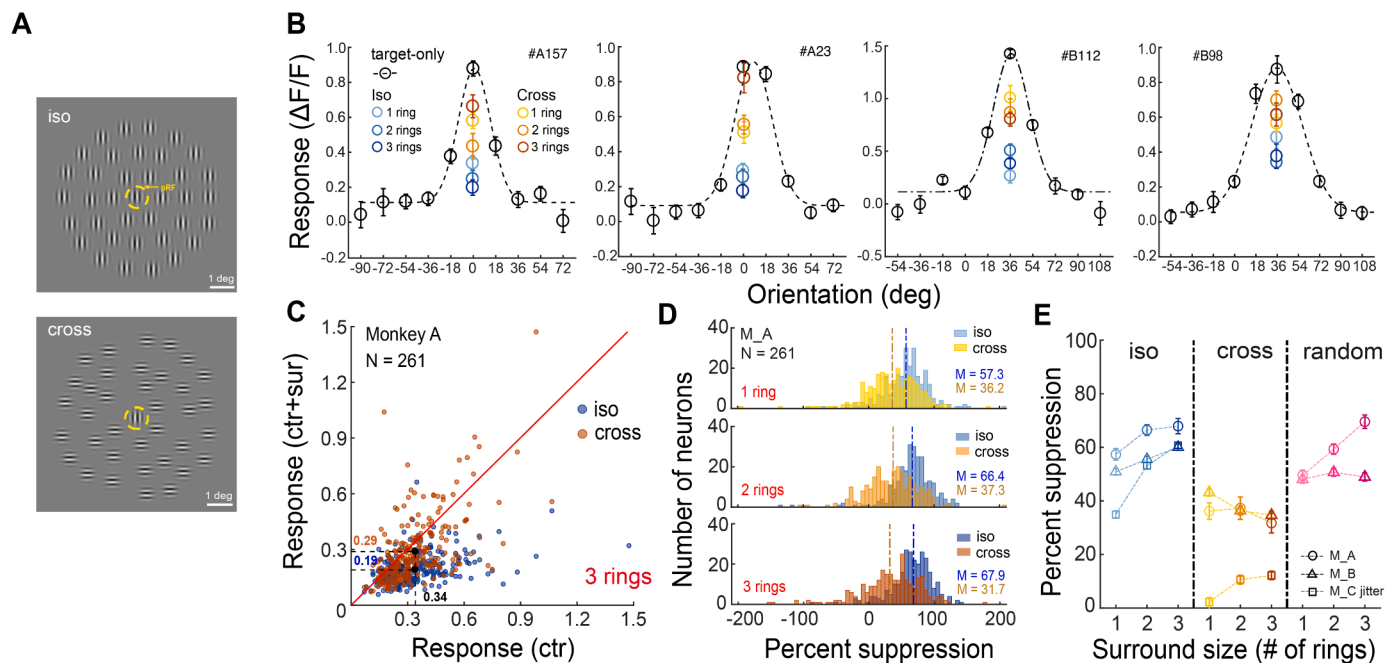


Fig. 2. Surround modulation of V1 neuronal responses. **A.** Center-surround stimuli. A high-contrast (0.90) Gabor target was placed in the population receptive field (pRF) of neurons, which in the current examples were surrounded by 3 rings of iso-oriented (upper) or cross-oriented (lower) Gabors. The pRF was outlined by a yellow dashed circle. **B.** Four exemplar neurons' orientation tuning functions measured with the central Gabor and the respective Gaussian fittings (Black circles and curves). The responses of each neuron at or near the preferred orientation were modulated by iso- and cross-surrounds of different sizes (1–3 rings) (colored circles). **C.** An exemplar scatterplot of responses of all center-orientation-tuned neurons with vs. without a 3-ring iso- or cross-surround from Monkey A. Mean responses were indicated by the black dots and dashed lines. **D.** The frequency distributions of percent suppression at iso- and cross-surrounds of different sizes in Monkey A. M: Mean. **E.** The mean percent suppression at various iso- and cross-surround conditions for three monkeys, as well as at random-surround conditions for Monkeys A and B. Error bars represent ± 1 SEM.

activities within a wide range of firing rates from 10 to 150 Hz (Li et al., 2017). During imaging, a $16 \times$ objective lens (0.8 N.A., Nikon) with a resolution of $1.6 \mu\text{m}/\text{pixel}$ was used, along with a 1000-nm femtosecond laser. A fast resonant scanning mode (32 fps) was chosen to obtain continuous images of neuronal activities (8 fps after averaging every 4 frames). The strength of fluorescent signals (mean luminance of a small area) was monitored and adjusted, if necessary, for the drift of fluorescent signals. One FOV of $850 \times 850 \mu\text{m}^2$ was selected for each animal.

2.5. Imaging data analysis: initial screening of ROIs

The data were analyzed using customized Matlab codes. A normalized cross-correlation-based translation algorithm was used to correct motion artifacts (Li et al., 2017). After the correction, fluorescence changes were associated with corresponding visual stimuli through the time sequence information recorded by a Neural Signal Processor (Cerebus system, Blackrock Microsystem). By subtracting the mean of the four frames before stimuli onset (F_0) from the average of the 5th–8th frames after stimuli onset (F) across 12–14 repeated trials for each stimulus condition, a differential image ($\Delta F = F - F_0$) was obtained.

For V1 FOVs in Monkeys A–C, regions of interest (ROIs) or possible cell bodies were determined by considering all stimuli conditions. ROIs were determined through sequential analysis of 190 differential images for each FOV, starting with 10 target-only conditions in which only a single Gabor was centered in the pRF at 10 orientations, followed by 180 center-surround conditions in which the central Gabor in the pRF was surrounded by 1–3 rings. More specifically, the 180 center-surround conditions were arranged in a $10 \times 3 \times 2(3) \times 2(3)$ order, including 10 center Gabor orientations, 3 surround sizes (1–3 surround rings), 2 or 3 surround orientations relative to the center stimulus (iso and cross surround orientations for Monkeys A–C, plus a random surround orientation for Monkeys A and B), and 2 or 3 absolute iso-/cross-surround orientations ($0^\circ/90^\circ$ and $36^\circ/126^\circ$ for Monkeys A–C, plus additional $18^\circ/108^\circ$ for Monkey C).

To select ROIs, the differential images were filtered with a band-pass Gaussian filter (size = 2–10 pixels), and connected subsets of pixels (>25 pixels, which would exclude smaller vertical neuropils) with the mean pixel value > 3 standard deviations of the mean brightness were selected as ROIs. Then, the areas of these ROIs were set to mean brightness in the next differential image before the bandpass filtering and thresholding were repeated. This measure would eventually reduce the SDs of differential images and facilitate the detection of neurons with relatively low fluorescence responses. If a new ROI and an existing ROI from the previous differential image overlapped, the new ROI would be on its own if the overlapping area $OA < 1/4 ROI_{\text{new}}$, discarded if $1/4 ROI_{\text{new}} < OA < 3/4 ROI_{\text{new}}$, and merged with the existing ROI if $OA > 3/4 ROI_{\text{new}}$. The merges would help smooth the contours of the final ROIs. This process went on through all 190 differential images twice to select ROIs. Finally, the roundness for each ROI was calculated as:

$$\text{Roundness} = \frac{\sqrt{4\pi \times A}}{P}$$

where A was an ROI's area, and P was the perimeter. Only ROIs with roundness larger than 0.9, which would exclude horizontal neuropils, were selected as neurons for further analysis.

2.6. Imaging data analysis: selection of orientation-tuned neurons

The ratio of fluorescence change ($\Delta F/F_0$) was calculated as a neuron's response to a specific stimulus condition. For a particular neuron's response to a stimulus condition, F_{0n} of the n -th trial was the average of 4 frames before stimulus onset, and F_n was the average of 5th–8th frames after stimulus onset (500–1000 ms). F_{0n} was then averaged across 12–14 repeated trials to obtain the baseline F_0 for all trials (to reduce noises in the calculation of responses), and $\Delta F_n/F_0 = (F_n - F_0)/F_0$ was taken as the neuron's response to this stimulus at the n -th trial.

To decide whether a neuron was orientation selective, each neuron's responses to a single Gabor at 10 orientations (drifting speed = 2 cycles/s, contrast = 0.9, SF = 6 cpd, and $\sigma = 0.142^\circ$) over 12–14 repeats were compared by performing a non-parametric Friedman test to test whether a neuron's responses at various orientations were significantly different from each other. The significance level was set at $\alpha = 0.01$ to reduce Type-I error. Neurons passing the Friedman test were selected as orientation-tuned neurons and were used for later analysis. Each neuron's orientation preference was equal to the Gabor orientation that elicited the maximal mean response amplitude over 12–14 repeats. The remaining ones were taken as non-orientation-tuned neurons.

2.7. The exclusion of neurons with their classical RFs intruded by surround stimuli

Neurons with their classical RFs intruded by surround stimuli were excluded from data analysis. To do so, neuronal responses to an inner-ring-only stimulus and to a blank screen were compared. Specifically, neuronal responses to the inner-ring stimulus after the stimulus onset (F) and to the blank screen (F_0) were collected for a total of 12–14 trials. Here the distance of an inner ring Gabor center to the stimulus center was approximately 0.96° . A non-parametric Friedman test was performed, which excluded neurons whose F was significantly different from F_0 ($p < 0.05$). The number of excluded neurons was 288 (29.9 %) for Monkey A, 214 (16.6 %) for Monkey B, and 212 (20.2 %) for Monkey C.

2.8. Model fitting and parameter estimation for population responses

The parameters (n , k) of the population gain-control model were estimated using the Matlab "lsqnonlin" function. The 95% CI for each parameter was derived from the covariance matrix of population responses. This matrix was computed using a regularized inverse approach, scaled by the mean square error of residuals (MSE), and was defined as:

$$\text{Cov}([n, k]) = \text{MSE} \cdot (\mathbf{J}^T \mathbf{J} + \lambda \mathbf{I})^{-1},$$

where \mathbf{J} was the Jacobian matrix, λ was the regularization parameter ($\lambda = 1 \times 10^{-4}$), and \mathbf{I} was the identity matrix with dimensions matching the number of parameters.

The 95% CIs for parameters (n , k) were calculated as:

$$SE_i = \sqrt{\text{diag}(\text{Cov}([n, k]))}, i \in \{n, k\}$$

$$CI_i = \hat{\theta}_i \pm 1.96 \cdot SE_i, \hat{\theta}_i \in \{\hat{n}, \hat{k}\},$$

where SE_i was the standard error for each parameter, and $\hat{\theta}_i$ denotes the estimated value of parameter i .

2.9. Model comparison for population tuning functions

To estimate the relative contributions of parameters n and k , we performed model comparisons using the Akaike Information Criterion corrected (AIC_c) for small sizes (Fernández et al., 2022). Assuming normally distributed errors and constant variance, AIC_c was calculated using the following equations (Burnham et al., 2002):

$$AIC = n \log(\hat{\sigma}^2) + 2k$$

$$\hat{\sigma}^2 = \frac{\sum \hat{E}_i^2}{n}$$

$$AIC_c = AIC + \frac{2k(k+1)}{n-k-1},$$

where n was the number of data points, k was the number of

parameters in the candidate model, and \hat{E}_i represented estimated residuals.

The differences in $AICc$ values ($\Delta AICc$) were used to compare the relative fitting performance between two single-parameter models. A smaller $\Delta AICc$ value would indicate that a specific single-parameter model approximates the two-parameter model more closely and that this specific parameter makes a greater contribution.

$$\Delta AIC_{c_i} = AIC_{c_i} - AIC_{c_{nk}}$$

2.10. Population coding of target orientation: linear discriminant analysis

To quantify the information loss in neuronal population regarding the center target orientation under iso- and cross-surround suppression, we calculated a population d' for each target orientation pair (0° vs. 36° and 90° vs. 126° for Monkeys A-B, and 18° vs. 36° and 108° vs. 126° for Monkeys C) using responses from all orientation-tuned neurons within an FOV whose receptive fields were not significantly intruded by the surround stimulus. Population d' characterized the distinguishability of neural response distributions to two sensory stimuli (Bishop, 2006), and the quantity $(d')^2$ served as a discrete analog of Fisher information (Averbeck and Lee, 2006).

To compute the population d' accurately despite having a substantially fewer number of trials than the number of cells recorded per FOV, we applied partial least squares discriminant analysis (PLS-DA) method to reduce V1 response dimensions by a procedure adapted from Rumyantsev et al. (2020). PLS-DA was implemented using the “*plsregress*” function in Matlab. For each target orientation pair, the V1 dataset was randomly split into “training” and “test” sets for 10-fold cross-validation. The “training” set was used to reduce the V1 population response dimensions and optimize the linear decoders defined by w_{opt} . The “test” set was used to compute the population d' of the optimal linear decoder under different surround conditions for each FOV. Linear decoders were optimized separately for each pair of target orientations under different surround conditions.

To reduce response dimensions, we projected the V1 neuronal population response matrix $R \in R^{N \times M}$ onto a truncated set of the N_R components identified by PLS-DA, where N was the number of orientation-tuned neurons for each FOV, and M ($M < N$) was the number of trials for each surround condition. For the target-only condition, N included 12–14 repeated trials for each target orientation. For iso- and cross-surround conditions, N included 3 types of surround sizes (1–3 surround rings) \times 12–14 repeated trials for each target orientation. Neural responses of each condition were z-scored before applying PLS analysis. After dimensionality reduction, the first two components ($N_R = 2$) of PLS were chosen for all subsequent determinations of d' , as adding further PLS components did not improve R^2 on test data sets in target-only and iso- and cross-surround conditions (Fig. 5A).

The population d' value of the optimal linear decoder in the two-dimensional population response space ($N_R = 2$) was calculated as (Rumyantsev et al., 2020):

$$(d'_{opt})^2 = \Delta\mu^T \Sigma^{-1} \Delta\mu = \Delta\mu^T w_{opt}$$

where $\Sigma = (\Sigma_A + \Sigma_B)/2$ was the noise covariance matrix averaged across two target orientations for each target orientation pair, $\Delta\mu = \mu_A - \mu_B$ was the vector difference between the mean neuronal population responses to two target orientations, and $w_{opt} = \Sigma^{-1} \Delta\mu$ was the optimal linear-decoding weight vector, which was normal to the optimal linear discrimination hyperplane in the population response space.

This entire procedure was repeated 20 times for each pair of target orientations, and the mean population d' averaged across two orientation pairs over 20 repetitions for each FOV was reported in Fig. 5A. By separately decoding neuronal population responses to different target orientation pairs, we provided an upper-bound estimate of the target information accessible to a linear readout strategy of the measured

responses.

2.11. Decoding contributions of individual neurons tuned to various orientations

Each neuron's decoding contribution was determined by a VIP (variable importance in projection) score (Chong and Jun, 2005). The VIP score was a summary of the variable importance in PLS analysis, calculated as a weighted sum of the squared correlations between the PLS components and the original variables, which were neuronal responses in this study. Neurons with VIP scores greater than 1 were considered significantly important for the PLS model's performance.

To quantify the aggregated decoding contributions of V1 neurons with different orientation preferences under target-only, iso-surround, and cross-surround conditions, we employed an attribution technique (Sundararajan et al., 2017). For each FOV and surround condition, neurons with similar orientation preferences were grouped in steps of 18° relative to one of the target orientations, resulting in 10 bins. To quantify the decoding contributions of each orientation bin, VIP scores of neurons within each bin were summed and normalized by the number of neurons. VIP scores of 10 orientation bins for two target orientation pairs were aligned and averaged for each FOV and surround condition, as shown in Fig. 5C. For each surround condition, we then calculated a population circular variance (CV) of the 10 orientation bins per FOV, using an equation adapted from Ringach et al. (2002):

$$CV = 1 - R = 1 - \frac{\sum_k r_k e^{i2\theta_k}}{\sum_k r_k},$$

where r_k was the normalized decoding weight of an orientation bin preferring the angles θ_k (θ_k spanned the range from 0 to 162° in steps of 18°). A population CV towards 0 would indicate high population orientation selectivity, while towards 1 would indicate low population orientation selectivity.

3. Results

V1 neuronal responses for iso- and cross-surround modulation were measured in three FOVs, one in each awake, fixating macaque. All three FOVs were located $\sim 200 \mu\text{m}$ deep from the cortical surface. Fig. 1C shows the time courses of calcium responses at different surround conditions from a FOV in Monkey A. A total of 3305 orientation-tuned neurons were identified from these images, accounting for 81.48 % of all identified V1 neurons. The functional maps of orientation-selective neurons are presented in Fig. 1D, which show orientation clusters as in a previous two-photon imaging study of ours (Ju et al., 2021). Among these neurons, 2591 (78.40 %) did not respond significantly to the inner surround-ring in the absence of the central target stimulus (see Materials and methods), suggesting that their receptive fields did not significantly overlap with the surround stimuli. Responses of these neurons to a central Gabor with 1–3 surround rings represent clean neuronal responses to surround modulation effects. Only these neurons were included in the subsequent analysis of surround modulation.

3.1. Individual neuronal response changes under surround modulation

Neuronal responses to a central target were measured under various surround conditions (Fig. 2A). Each iso- or cross-surround consisted of 1–3 circular rings of Gabor elements with the ring radii at 0.96° , 1.92° , and 2.88° , respectively. The surround was position-jittered randomly trial by trial within $\pm 0.12^\circ$ in the x and y directions as a whole in Monkeys A-B, and within 0.36° in the x and y directions in Monkey C. In addition, the surround elements were also individually randomly oriented (Monkeys A & B only). The central and surround Gabors were identical except that the orientations were not always the same.

As shown in four example neurons (Fig. 2B), neuronal responses to the central Gabor at the preferred orientation were suppressed by surround stimuli, but the suppression was reduced with cross-surrounds, consistent with previous reports (Knierim and van Essen, 1992; Kastner et al., 1997; Schmid et al., 2014; Yan et al., 2018). Furthermore, following Cavanaugh et al. (2002b), we calculated each neuron's center selectivity index: $(R_{\text{opt}} - R_{\text{orth}})/(R_{\text{opt}} + R_{\text{orth}})$ and surround selectivity index: $(R_{\text{cross}} - R_{\text{iso}})/(R_{\text{cross}} + R_{\text{iso}})$, where R_{opt} and R_{orth} were a neuron's respective responses to the center Gabor at the preferred and orthogonal orientations, and R_{cross} and R_{iso} were the neuron's respective responses to the center Gabor at the preferred orientation under cross- and iso-surround suppression. These neurons' center selectivity indices were 0.91, 0.77, 1.12, and 0.93, respectively, larger than the corresponding 3-ring surround selectivity indices at 0.54, 0.65, 0.36, and 0.24, again consistent with previous reports (Li and Li, 1994; Cavanaugh et al., 2002b).

At a large scale, for all center orientation-tuned neurons in the FOV of Monkey A, iso-surrounds reduced the peak responses to the central target more than cross-surrounds did in terms of percent suppression (calculated as $(R_c - R_{c+s})/R_c \times 100\%$, in which R_c and R_{c+s} were a neuron's respective responses to the central target only and with a surround) (Fig. 2C and D). The same trends were observed in all three monkeys (Fig. 2E). We performed a mixed-design ANOVA with surround orientation (iso vs. cross) and surround size (number of rings) as within-subject factors and monkey (Monkeys A-C) as a between-subject factor, which confirmed a significant main effect of surround orientation ($F_{1, 961} = 461.12, p < 0.001$) in all three monkeys. A post-hoc analysis with Bonferroni correction further revealed that iso-surround suppression

strengthened with larger surround size ($ps < 0.001$ for 1 ring vs. 2 rings, 2 rings vs. 3 rings, and 1 ring vs. 3 rings), but cross-surround suppression did not show significant change ($ps \geq 0.855$ for 1 ring vs. 2 rings, 2 rings vs. 3 rings, and 1 ring vs. 3 rings). Moreover, random-surrounds appeared to produce as much suppression as iso-surrounds did in Monkeys A and B (Fig. 2E). Additionally, we also compared the percent of surround suppression when the center-surround orientation contrast increased from 0° to 162° in steps of 18° . The results showed decreased surround suppression as the center-surround orientation contrast increased (Fig. S2).

3.2. Population orientation tuning functions under surround modulation

We were particularly interested in the impacts of iso- and cross-surrounds on population orientation tuning functions, which considered the responses of all orientation-tuned neurons and thus provided a more complete assessment of surround modulation. Population orientation tuning functions with different surround conditions were constructed following the procedure in Busse et al. (2009). Specifically, neurons with similar orientation preferences were binned (bin width: 18°) relative to the target orientation for a total of 10 bins, and the resultant population orientation tuning functions based on the mean responses of these bins were fitted with a Gaussian function (Fig. 3A).

Similar to individual neuronal data (Fig. 2), the population responses of neurons best-tuned to the center stimulus orientation were suppressed more by iso- and random-surrounds than by cross-surrounds. What was not discernable from individual results was that neurons tuned to all orientations, including orthogonal orientations, were suppressed by iso-

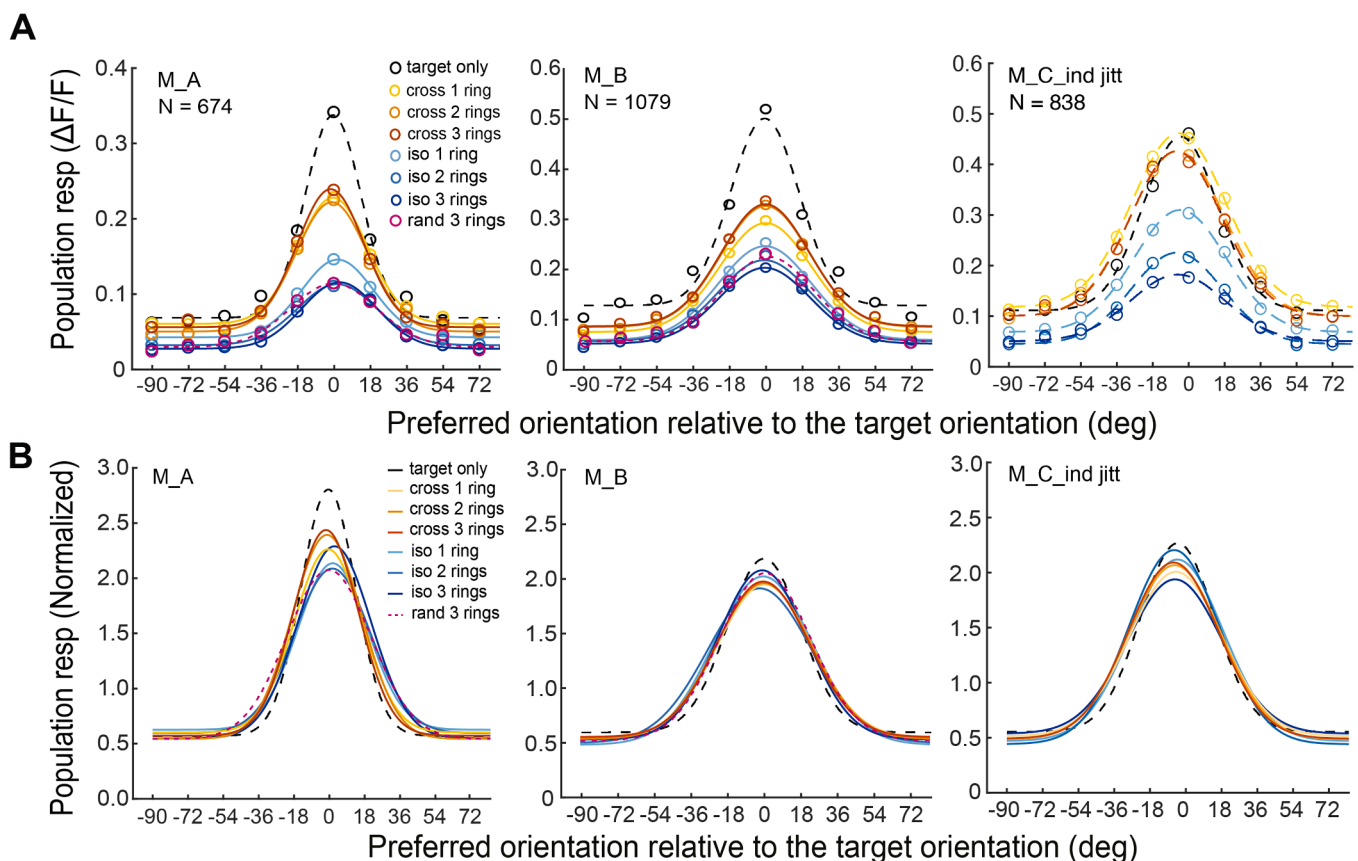


Fig. 3. Population responses under surround modulation. A. Population orientation tuning functions with the target-only condition and various iso- and cross-surround conditions. A population function with the random surround at a size of 3 rings (pink dotted line) was also shown in the FOVs of Monkeys A and B, respectively. Functions of the other two sizes were not shown for clarity. Neurons with similar orientation preferences were grouped in 18° bins. Black and colored dots were the mean responses of each bin. Curves were best fitting Gaussians ($R^2 > 0.98$). B. The above population orientation tuning functions normalized by respective means.

and random-surrounds, suggesting an orientation-unspecific component of surround suppression. Further, when population functions were normalized by respective means to discount orientation-unspecific iso-surround suppression (Fig. 3B), the remaining orientation-specific iso-surround suppression appeared to be a lesser effect, indicating stronger orientation-unspecific than specific suppression by iso-surrounds. On the other hand, equally conspicuous, the normalized population functions under iso/random- and cross-surround conditions were similar, especially in the average sense (cross-surround functions tended to be slightly higher than iso-surround functions in Monkey A, similar in Monkey B, and slightly lower in Monkey C, Fig. 3B). Therefore, the cross-surround effects may mostly reflect a reduction of orientation-unspecific surround suppression by a scaling factor.

To quantify the above observations, we employed a simple population gain control model to fit the population orientation tuning functions under surround modulation: $R_{c+s} = R_c^n/k$. Here, R_c represented the Gaussian-fitted population orientation tuning function under target-only conditions (180 data points for neuronal responses across $[-90, 90]^\circ$), and R_{c+s} represented the population orientation tuning functions under surround modulation. The free parameter n varied the slope of the input population orientation tuning function, so its impact was orientation-specific. The free parameter k was the orientation-unspecific divisive gain control factor that represented general orientation-unspecific surround suppression.

The model fitted the population orientation tuning functions under surround modulation very well (all $R^2 > 0.98$) (Fig. 4A). The slope parameter n was substantially lower than 1 in Monkey A, but showed less difference or sometimes no difference in the other two monkeys

(Fig. 4B; Notice that the error bars here are 95 % CIs), while the gain parameter k was larger than 1 (except for Monkey C with cross-surrounds) and consistently higher with iso/random-surrounds than with cross-surrounds (Fig. 4C). These parameter changes confirmed that surround modulation consists of an orientation-specific component, which reduces the slope and broadens the bandwidth of input population orientation tuning (as $n < 1$ in most cases). It also consisted of an orientation-unspecific suppression component (as $k > 1$), with more suppression from iso/random surrounds than from cross-surrounds ($k_{iso/random} > k_{cross}$). Moreover, because $n_{iso} \approx n_{cross}$ and $k_{cross} < k_{iso}$, the weaker suppression by cross-surrounds was mainly a result of orientation-unspecific gain change.

Furthermore, we performed model comparisons using the Akaike Information Criterion corrected ($AICc$) for small sizes (Burnham et al., 2002) to assess the relative contributions of two parameters in the model to population surround modulation (see Materials and methods). We calculated the differences in $AICc$ scores ($\Delta AICc$) between the above two-parameter model ($AICc_{nk}$) and each of the two single-parameter models ($AICc_n$ & $AICc_k$) that let either n or k vary with the other one fixed at 1 to be ineffective. Here, a smaller $\Delta AICc$ would suggest a great contribution. For the two-parameter model, the respective mean $AICc_{nk}$ averaged over 1–3 surround rings and all FOVs was -1684.65 and -1542.60 under iso and cross surrounds. Meanwhile, for the single-parameter models, when n was varied, the respective mean $AICc_n$ for iso and cross surrounds were -1122.70 and -1218.57 . Therefore, $\Delta AICc_n$ ($\Delta AICc_n = AICc_n - AICc_{nk}$) was 561.95 and 324.02 for iso and cross surrounds, respectively. In contrast, when k was varied, the respective mean $AICc_k$ for iso and cross surrounds was -1581.50 and

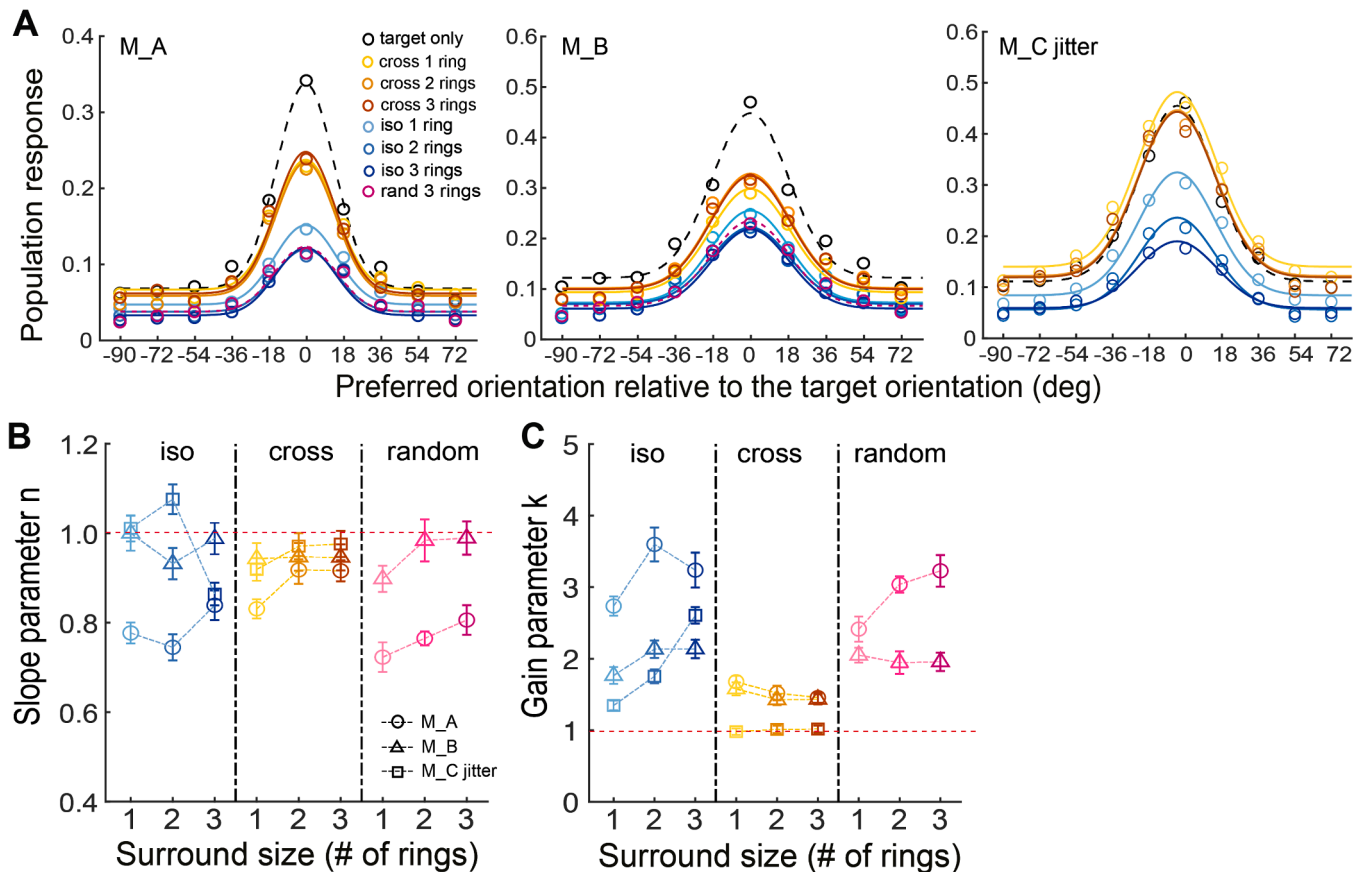


Fig. 4. A population gain control model of surround modulation. A. Model-predicted population orientation-tuning functions with various surround conditions for each macaque. The black and colored circles were the mean responses of each group of neurons with various orientation preferences. The black curve was the best fitting Gaussian for the target-only condition (same as Fig. 3A), serving as the model input, and the colored curves were model-predicted population orientation-tuning functions under iso-, cross-, and random-surround conditions. B. The slope parameter n under various surround conditions. C. The gain parameter k under various surround conditions. Error bars represent 95 % CI.

-1462.51, and the corresponding mean ΔAIC_{C_k} ($\Delta AIC_{C_k} = AIC_{C_k} - AIC_{C_{nk}}$) was 103.15 and 80.08 for iso and cross surrounds. These results thus confirm that surround modulation is predominantly driven by orientation-unspecific gain changes (k) than by orientation-specific slope or bandwidth changes (n).

3.3. Population coding of target orientation under surround modulation

The representation of stimulus features in V1 arises not only from individual neuronal responses but also from population-level activities (Cunningham and Yu, 2014). The underlying structures of population responses and related variability in neuronal responses can be revealed

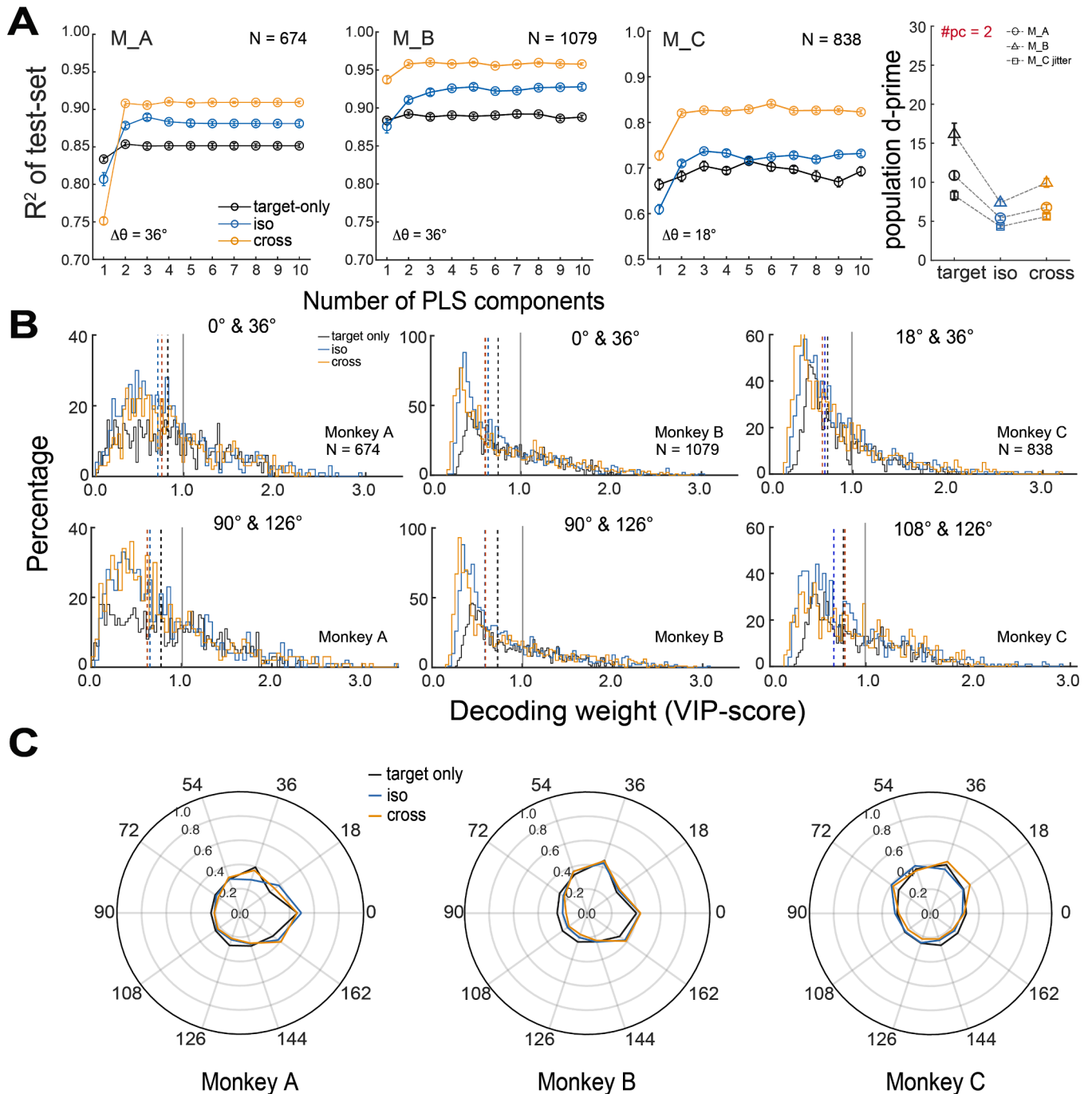


Fig. 5. V1 population coding of the center stimulus orientation under surround suppression. A. Left: The mean goodness-of-fits (R^2) of PLS models on test datasets averaged over two target orientation pairs with an increasing number of PLS components. The orientation difference of the two target stimuli was 36° for Monkeys A and B and 18° for Monkey C. Right: Mean population d' values under various surround conditions for Monkeys A-C. For each condition, the population d' values were averaged over two target orientation pairs with a 36° separation (0° vs. 36° and 90° vs. 126°) for Monkeys A-B, and with an 18° separation (18° vs. 36° and 108° vs. 126°) for Monkey C. Error bars represent ± 1 SEM. B. Frequency distributions of V1 neuronal VIP scores of the optimized PLS model under various surround conditions in Monkeys A-C. C. Decoding contributions of V1 neurons with various orientation preferences. Neurons with similar orientation preferences were binned in steps of 18° and aligned to the center target's orientation. Neurons at 0° & 36° of the polar coordinates for Monkeys A and B, and at 0° & 18° for Monkey C, are those tuned to the orientations of target stimulus pairs. Color lines indicate the aggregated decoding contributions for each orientation bin averaged across two target orientation pairs under three surround conditions.

through methods of dimensionality reduction, as shown in Fig. 5A. We examined V1 population coding of target orientation under various surround conditions to determine: (1) the loss of target orientation information due to iso- and cross-surround suppression, and (2) the contributions of neurons with various orientation preferences to population coding under surround suppression.

To assess the loss of target orientation information under surround modulation, we analyzed the orientation discriminability of the central target based on V1 population responses using a linear discriminant analysis adapted from Rumyantsev et al. (2020). For each surround condition, we used the population discriminability index (d') to determine how well two pairs of target orientations (0° vs. 36° and 90° vs. 126° for Monkeys A & B, and 18° vs. 36° and 108° vs. 126° for Monkey C) could be distinguished by using response from all orientation-tuned neurons. To determine d' accurately despite having far fewer trials than cells recorded per FOV, we applied partial least squares (PLS) analysis for dimensional reduction (see Materials and methods). The first two components were sufficient to distinguish the stimulus pairs effectively (Fig. 5A left three panels). Next, we optimized linear decoders separately for each target pair based on the first two PLS components. The population d' value of the optimal linear decoder was then calculated for each target orientation pair (Fig. 5A right panel) (see Materials and methods). The results showed that V1 neurons can effectively discriminate the 36° (Monkeys A-B) or 18° (Monkey C) orientation differences of stimulus pairs under all conditions. Nevertheless, compared to the target-only condition, iso- and cross-surround suppression resulted in a loss of center stimulus orientation information in all three monkeys, as indicated by the reduced d' values (Fig. 5A far right panel), which was more substantial with iso-surrounds than with cross-surrounds.

To further understand the effects of surround suppression on the population coding structure in V1 neurons, we examined how individual neurons contributed to the population decoding of center target orientation. For each surround condition, the individual neuronal decoding contribution was determined by a VIP score (variable importance in projection) (see Materials and methods), which summarized the variable importance in PLS discriminant analysis (Chong and Jun, 2005). Neurons with VIP scores above 1 were considered significantly important in the population coding of target orientation. Fig. 5B shows the frequency distributions of VIP scores for the PLS discriminant analysis under three surround conditions for each FOV. The frequency distributions of VIP scores were right-skewed. Only 35.2 %, 28.6 %, and 30.5 % of the orientation-tuned neurons had VIP scores > 1 for target-only, iso-surround, and cross-surround conditions averaged across three FOVs, in which the percentages with iso- and cross-surround conditions were lower than those with the target-only condition. These results suggest that fewer neurons made significant contributions to the decoding of stimulus orientation under surround suppression, particularly with iso-surrounds.

Furthermore, we analyzed the decoding contributions of V1 neurons with various orientation preferences (see Materials and methods). Fig. 5C shows the aggregated decoding contributions of various orientation bins for Monkeys A-C, respectively. A population circular variance (CV) was then calculated for each condition to quantify the variability in decoding contributions across the various orientation bins (see Materials and Methods). A population CV close to 0 indicates high orientation selectivity, and close to 1 indicates low orientation selectivity. The mean population circular variances for target-only, iso-surround, and cross-surround conditions were 0.88, 0.83, and 0.82 for Monkey A, 0.86, 0.81, and 0.77 for Monkey B, and 0.89, 0.86, and 0.82 for Monkey C, respectively. These high population CV values indicate predominantly orientation-unspecific decoding contributions from V1 neurons, supporting our earlier conclusion regarding predominantly orientation-untuned surround suppression.

4. Discussion

The population orientation tuning function data reveal that iso-surrounds produce predominantly orientation-unspecific suppression to neurons tuned to all orientations, with additional weak suppression to neurons tuned to the center stimulus orientation. Moreover, cross-surrounds mainly reduce orientation-unspecific suppression by scaling up the responses of all neurons. These results suggest that the orientation specificity of surround modulation observed in previous single-unit studies is actually part of largely orientation-unspecific population response changes, which is describable by a population gain control model. Further population analyses support these conclusions by demonstrating that surround suppression is associated with fewer neurons contributing to population orientation coding and that these contributing neurons have diverse orientation preferences.

In various theories and models, surround suppression is generated when iso-surrounds activate inhibitory neurons through orientation-specific long-range horizontal connections to suppress neuronal responses (Li, 1999; Kapadia et al., 2000; Stettler et al., 2002). Further, horizontal connections may also be responsible for orientation-unspecific suppression. For example, Angelucci et al. (2017) proposed that horizontal connections also connect to inhibitory basket neurons, which in turn target neurons tuned to other orientations to produce orientation-untuned suppression. Similarly, the stabilized supralinear network model (Rubin et al., 2015; Holt et al., 2024) suggests that long-range horizontal connections activate the local network involving multiple orientation columns, which engages short-range interactions to strengthen the inhibitory feedback across all neurons in the local network, resulting in suppression of all neurons regardless of their orientation preferences. However, qualitatively, these models do not necessarily predict predominantly orientation-unspecific suppression of population orientation responses by iso-surrounds, as both orientation-specific and unspecific surround effects are supposedly initiated through orientation-specific long-range horizontal connections. They may also have more difficulty predicting nearly equal suppression by iso- and random-surrounds either, as random-surrounds are not expected to produce as much orientation-specific suppression through orientation-specific horizontal connections. Furthermore, these models cannot predict reductions of mostly orientation-unspecific suppression by cross-surrounds either, as removing orientation-specific long-range influences associated with iso-surrounds would reduce both orientation-specific and unspecific suppression. Therefore, these existing models of surround modulation face challenges from major population response characteristics our study reveals.

Largely orientation-unspecific suppression by iso- and random-surrounds may instead be more consistent with recent reports that V1 horizontal connections target heterogeneous orientation domains, especially at longer distances beyond the classical receptive field (Chavane et al., 2011; Huang et al., 2014; Martin et al., 2014; Omer et al., 2019; Ju et al., 2020), although more homogeneous orientation-specific connections are also reported by other studies (Gerard-Mercier et al., 2016; Chernov et al., 2018). As mentioned earlier, one of our labs used high-resolution two-photon imaging to measure the precise orientation inputs on different spots of the dendrite trees of macaque V1 superficial-layer neurons (Ju et al., 2020). They found that the orientation inputs the neurons receive are heterogeneous, in that locally clustered inputs at different dendrite tree spots represent different orientation domains. Nevertheless, the integrated orientation preference of dendritic inputs is close to the neuron's orientation preference. These dendrite imaging results thus may to some degree reconcile conflicting conclusions regarding the homogeneity or heterogeneity of horizontal connections among studies, but it still suggests a large and diverse range of orientation inputs and thus predominantly orientation-unspecific surround effects.

Surround modulation is often described as divisive inhibition in gain-control models which balances neural excitation through normalization

(Heeger, 1992; Webb et al., 2005; Carandini and Heeger, 2013; Angelucci et al., 2017; Li et al., 2022). If surround modulation is indeed orientation-specific, an orientation-dependent component of divisive inhibition needs to be included in the model. This is exemplified by the model proposed by Angelucci et al. (2017), which incorporates long-range horizontal connections to account for observed orientation-specific suppression in the near surround, while the more extended far-surround modulation may result from top-down feedback (Shushruth et al., 2012). However, our modeling results suggest that surround modulation can be effectively represented by a simple scaling factor, $1/k$, which reflects orientation-unspecific divisive inhibition, similar to the divisive inhibition within the classical receptive field as described in Heeger's original model that pools the responses of neurons tuned to all orientations (Heeger, 1992). It is also consistent with the original proposal that surround suppression operates similarly to divisive inhibition within the classical receptive field, merely extending the extent of the suppressive field (Carandini and Heeger, 2013).

The orientation-specific component of suppression is largely unchanged with iso-, cross, and even random surrounds. We suspect that this orientation-specific surround suppression may result from the response nonlinearity of best-tuned neurons under the influence of general surround effects, as evidenced by the largely stable slope parameter n in the population gain control model (Fig. 4B). On the other hand, predominantly orientation-unspecific suppression reduction by cross-surrounds may be a result of orientation discontinuity, to which neuronal responses are enhanced even when a neuron is not stimulated by an optimally oriented stimulus (Sillito et al., 1995; Shushruth et al., 2012), though no super-facilitation is evident in our population results. This upscaling effect may originate from higher visual areas via feedback (Sillito et al., 1995; Shushruth et al., 2012), as well as from local cross-orientation facilitation from V1 plaid neurons (Guan et al., 2020). Consequently, the orientation-unspecific surround suppression is reduced while the orientation-specific suppression remains largely intact. In addition, the changes of the cross effects with the surround size are flatter than those of the iso effects in all three monkeys (Fig. 2E), suggesting that the spatial extents of cross facilitation in these monkeys are at least as large as those of iso suppression.

Finally, a technical note: We employed a population RF approach and did not measure the exact RF of each ROI. However, the identified neurons most likely had their RFs overlapping with the stimulus, resulting in significant responses. A recent two-photon imaging study (Nauhaus et al., 2016) reported that the RF scatter in V1 was approximately half of the originally estimate by Hubel and Wiesel (1974). Our own detailed RF mapping data in a separate macaque also suggest that the RF scatters of superficial-layer V1 neurons have very narrow distributions (vertical and horizontal standard deviations both $< 0.15^\circ$) (Fig. S3). Hence, our measurements likely captured most neurons that could be triggered by the stimuli. There may have been some neurons whose RFs did not align well with the stimulus and thus exhibited weak and orientation-unspecific responses. These neurons would have been filtered out through data analysis (see Materials and methods).

CRediT authorship contribution statement

Zhao Xing-Nan: Writing – original draft, Formal analysis, Data curation. **Zhang Sheng-Hui:** Formal analysis, Data curation. **Tang Shi-Ming:** Writing – review & editing, Methodology. **Yu Cong:** Writing – review & editing, Formal analysis, Conceptualization.

Declaration of Competing Interest

The authors declare no conflict of interest.

Acknowledgments

This study was supported by a Ministry of Science and Technology,

China, STI2030-Major Projects grant (2022ZD0204600), Natural Science Foundation of China grants (31230030 and 31730109), and funds from Peking-Tsinghua Center for Life Sciences, Peking University.

Appendix A. Supporting information

Supplementary data associated with this article can be found in the online version at [doi:10.1016/j.pneurobio.2025.102745](https://doi.org/10.1016/j.pneurobio.2025.102745).

Data availability

Data will be made available on request.

References

- Adesnik, H., Bruns, W., Taniguchi, H., Huang, Z.J., Scanziani, M., 2012. A neural circuit for spatial summation in visual cortex. *Nature* 490, 226–231.
- Angelucci, A., Bijnanzadeh, M., Nurminen, L., Federer, F., Merlin, S., Bressloff, P.C., 2017. Circuits and mechanisms for surround modulation in visual cortex. *Annu. Rev. Neurosci.* 40 (40), 425–451.
- Averbeck, B.B., Lee, D., 2006. Effects of noise correlations on information encoding and decoding. *J. Neurophysiol.* 95, 3633–3644.
- Bishop, C.M., 2006. *Pattern Recognition and Machine Learning*. Springer, New York.
- Blakemore, C., Tobin, E.A., 1972. Lateral inhibition between orientation detectors in the cat's visual cortex. *Exp. Brain Res* 15, 439–440.
- Bosking, W.H., Zhang, Y., Schofield, B., Fitzpatrick, D., 1997. Orientation selectivity and the arrangement of horizontal connections in tree shrew striate cortex. *J. Neurosci.* 17, 2112–2127.
- Burnham, K.P., Anderson, D.R., & Burnham, K.P. (2002). *Model selection and multimodel inference: a practical information-theoretic approach* (2nd ed.). New York: Springer.
- Busse, L., Wade, A.R., Carandini, M., 2009. Representation of concurrent stimuli by population activity in visual cortex. *Neuron* 64, 931–942.
- Carandini, M., & Heeger, D.J. (2013). Normalization as a canonical neural computation (vol 13, pg 51, 2012). *Nature Reviews Neuroscience*, 14, 152–152.
- Cavanaugh, J.R., Bair, W., Movshon, J.A., 2002a. Nature and interaction of signals from the receptive field center and surround in macaque V1 neurons. *J. Neurophysiol.* 88, 2530–2546.
- Cavanaugh, J.R., Bair, W., Movshon, J.A., 2002b. Selectivity and spatial distribution of signals from the receptive field surround in macaque V1 neurons. *J. Neurophysiol.* 88, 2547–2556.
- Chavane, F., Sharon, D., Jancke, D., Marre, O., Fregnac, Y., Grinvald, A., 2011. Lateral Spread of Orientation Selectivity in V1 is Controlled by Intracortical Cooperativity. *Front Syst. Neurosci.* 5, 4.
- Chen, C.C., Tyler, C.W., 2002. Lateral modulation of contrast discrimination: flanker orientation effects. *J. Vis.* 2, 520–530.
- Chernov, M.M., Friedman, R.M., Chen, G., Stoner, G.R., Roe, A.W., 2018. Functionally specific optogenetic modulation in primate visual cortex. *Proc. Natl. Acad. Sci. USA* 115, 10505–10510.
- Chong, I.-G., Jun, C.-H., 2005. Performance of some variable selection methods when multicollinearity is present. *Chemom. Intell. Syst. Syst.* 78, 103–112.
- Cunningham, J.P., Yu, B.M., 2014. Dimensionality reduction for large-scale neural recordings. *Nat. Neurosci.* 17, 1500–1509.
- DeAngelis, G.C., Freeman, R.D., Ohzawa, I., 1994. Length and width tuning of neurons in the cat's primary visual cortex. *J. Neurophysiol.* 71, 347–374.
- Fernández, A., Okun, S., Carrasco, M., 2022. Differential effects of endogenous and exogenous attention on sensory tuning. *J. Neurosci.* 42, 1316–1327.
- Gerard-Mercier, F., Carelli, P.V., Pananceu, M., Troncoso, X.G., Fregnac, Y., 2016. Synaptic correlates of low-level perception in V1. *J. Neurosci.* 36, 3925–3942.
- Gilbert, C.D., 1977. Laminar differences in receptive field properties of cells in cat primary visual cortex. *J. Physiol.* 268, 391–421.
- Gilbert, C.D., Das, A., Ito, M., Kapadia, M., Westheimer, G., 1996. Spatial integration and cortical dynamics. *Proc. Natl. Acad. Sci. USA* 93, 615–622.
- Gilbert, C.D., Wiesel, T.N., 1989. Columnar specificity of intrinsic horizontal and corticocortical connections in cat visual cortex. *J. Neurosci.* 9, 2432–2442.
- Guan, S.C., Ju, N., Tao, L., Tang, S.M., Yu, C., 2021. Functional organization of spatial frequency tuning in macaque V1 revealed with two-photon calcium imaging. *Prog. Neurobiol.* 205, 102120.
- Guan, S.C., Zhang, S.H., Zhang, Y.C., Tang, S., Yu, C., 2018. Plaid detectors in macaque V1 revealed by two-photon calcium imaging. *Curr. Biol.* 30, 934–940.
- Guan, S.C., Zhang, S.H., Zhang, Y.C., Tang, S., Yu, C., 2020. Plaid detectors in macaque V1 revealed by two-photon calcium imaging. *Curr. Biol.* 30, 934–940.
- Heeger, D.J., 1992. Normalization of cell responses in cat striate cortex. *Vis. Neurosci.* 9, 181–197.
- Holt, C.J., Miller, K.D., Ahmadian, Y., 2024. The stabilized supralinear network accounts for the contrast dependence of visual cortical gamma oscillations. *PLoS Comput. Biol.* 20, e1012190.
- Huang, X., Elyada, Y.M., Bosking, W.H., Walker, T., Fitzpatrick, D., 2014. Optogenetic assessment of horizontal interactions in primary visual cortex. *J. Neurosci.* 34, 4976–4990.
- Hubel, D.H., Wiesel, T.N., 1965. Receptive fields and functional architecture in two nonstriate visual areas (18 and 19) of the cat. *J. Neurophysiol.* 28, 229–289.

- Hubel, D.H., Wiesel, T.N., 1974. Uniformity of monkey striate cortex: a parallel relationship between size, scatter, and magnification factor. *J. Comp. Neurol.* 158, 295–305.
- Ju, N.S., Guan, S.C., Tao, L., Tang, S.M., Yu, C., 2021. Orientation tuning and end-stopping in macaque V1 studied with two-photon calcium imaging. *Cereb. Cortex* 31, 2085–2097.
- Ju, N.S., Li, Y., Liu, F., Jiang, H., Macknik, S.L., Martinez-Conde, S., Tang, S., 2020. Spatiotemporal functional organization of excitatory synaptic inputs onto macaque V1 neurons. *Nat. Commun.* 11, 697.
- Kapadia, M.K., Westheimer, G., Gilbert, C.D., 2000. Spatial distribution of contextual interactions in primary visual cortex and in visual perception. *J. Neurophysiol.* 84, 2048–2062.
- Kastner, S., Nothdurft, H.C., Pigarev, I.N., 1997. Neuronal correlates of pop-out in cat striate cortex. *Vis. Res* 37, 371–376.
- Knierim, J.J., van Essen, D.C., 1992. Neuronal responses to static texture patterns in area V1 of the alert macaque monkey. *J. Neurophysiol.* 67, 961–980.
- Li, Z., 1999. Contextual influences in V1 as a basis for pop out and asymmetry in visual search. *Proc. Natl. Acad. Sci. USA* 96, 10530–10535.
- Li, C.Y., Li, W., 1994. Extensive integration field beyond the classical receptive field of cat's striate cortical neurons—classification and tuning properties. *Vis. Res* 34, 2337–2355.
- Li, M., Liu, F., Jiang, H., Lee, T.S., Tang, S., 2017. Long-term two-photon imaging in awake Macaque Monkey. *Neuron* 93, 1049–1057 e1043.
- Li, Y., Wang, T., Yang, Y., Dai, W., Wu, Y., Li, L., Xing, D., 2022. Cascaded normalizations for spatial integration in the primary visual cortex of primates. *Cell Rep.* 40, 111221.
- Malach, R., Amir, Y., Harel, M., Grinvald, A., 1993. Relationship between intrinsic connections and functional architecture revealed by optical imaging and in vivo targeted biocytin injections in primate striate cortex. *Proc. Natl. Acad. Sci. USA* 90, 10469–10473.
- Martin, K.A., Roth, S., Rusch, E.S., 2014. Superficial layer pyramidal cells communicate heterogeneously between multiple functional domains of cat primary visual cortex. *Nat. Commun.* 5, 5252.
- Nauhaus, I., Nielsen, K.J., Callaway, E.M., 2016. Efficient receptive field tiling in primate V1. *Neuron* 91, 893–904.
- Omer, D.B., Fekete, T., Ulchin, Y., Hildesheim, R., Grinvald, A., 2019. Dynamic patterns of spontaneous ongoing activity in the visual cortex of anesthetized and awake monkeys are different. *Cereb. Cortex* 29, 1291–1304.
- Pelli, D.G., Zhang, L., 1991. Accurate control of contrast on microcomputer displays. *Vis. Res* 31, 1337–1350.
- Polat, U., Sagi, D., 1993. Lateral interactions between spatial channels: suppression and facilitation revealed by lateral masking experiments. *Vis. Res* 33, 993–999.
- Ringach, D.L., Shapley, R.M., Hawken, M.J., 2002. Orientation selectivity in macaque V1: diversity and laminar dependence. *J. Neurosci.* 22, 5639–5651.
- Rubin, D.B., Van Hooser, S.D., Miller, K.D., 2015. The stabilized supralinear network: a unifying circuit motif underlying multi-input integration in sensory cortex. *Neuron* 85, 402–417.
- Rumyantsev, O.I., Lecoq, J.A., Hernandez, O., Zhang, Y., Savall, J., Chrapkiewicz, R., Schnitzer, M.J., 2020. Fundamental bounds on the fidelity of sensory cortical coding. *Nature* 580, 100–105.
- Schmid, A.M., Purpura, K.P., Victor, J.D., 2014. Responses to orientation discontinuities in V1 and V2: physiological dissociations and functional implications. *J. Neurosci.* 34, 3559–3578.
- Shushruth, S., Mangapathy, P., Ichida, J.M., Bressloff, P.C., Schwabe, L., Angelucci, A., 2012. Strong recurrent networks compute the orientation tuning of surround modulation in the primate primary visual cortex. *J. Neurosci.* 32, 308–321.
- Sillito, A.M., Grieve, K.L., Jones, H.E., Cudeiro, J., Davis, J., 1995. Visual cortical mechanisms detecting focal orientation discontinuities. *Nature* 378, 492–496.
- Stettler, D.D., Das, A., Bennett, J., Gilbert, C.D., 2002. Lateral connectivity and contextual interactions in macaque primary visual cortex. *Neuron* 36, 739–750.
- Sundararajan, M., Taly, A., Yan, Q.Q., 2017. Axiomatic attribution for deep networks. *Int. Conf. Mach. Learn.* 70, 70.
- Webb, B.S., Dhruv, N.T., Solomon, S.G., Tailby, C., Lennie, P., 2005. Early and late mechanisms of surround suppression in striate cortex of macaque. *J. Neurosci.* 25, 11666–11675.
- Yan, Y., Zhaoping, L., Li, W., 2018. Bottom-up saliency and top-down learning in the primary visual cortex of monkeys. *Proc. Natl. Acad. Sci. USA* 115, 10499–10504.
- Yu, C., Klein, S.A., Levi, D.M., 2003. Cross- and iso-oriented surrounds modulate the contrast response function: the effect of surround contrast. *J. Vis.* 3, 527–540.
- Yu, C., Levi, D.M., 2000. Surround modulation in human vision unmasked by masking experiments. *Nat. Neurosci.* 3, 724–728.